J Mol Model (2013) 19:4003–4012
DOI 10.1007/s00894-013-1932-7

ORIGINAL PAPER

Spin-flip reactions of Zr + C_2H_6 researched by relativistic density functional theory

Yi Xiao · Xian-Yang Chen · Yi-Xiang Qiu · Shu-Guang Wang

Received: 30 January 2013 / Accepted: 19 June 2013 / Published online: 13 July 2013

Abstract Density functional theory (DFT) with relativistic corrections of zero-order regular approximation (ZORA) has been applied to explore the reaction mechanisms of ethane dehydrogenation by Zr atom with triplet and singlet spin-states. Among the complicated minimum energy reaction path, the available states involves three transition states (**TS**), and four stationary states (**1**) to (**4**) and one intersystem crossing with spin-flip (marked by ⇒): ^{3}Zr + C_2H_6 → ^{3}Zr-CH_3-CH_3 (^{3}**1**) → ^{3}**TS$_{1/2}$** → ^{3}ZrH-CH_2-CH_3 (^{3}**2**) → ^{3}**TS$_{2/3}$** ⇒ ^{1}ZrH_2-CH_2 = CH_2 (^{1}**3**) → ^{1}**TS$_{3/4}$** → ^{1}ZrH_3-CH = CH_2 (^{1}**4**). The minimum energy crossing point is determined with the help of the DFT fractional-occupation-number (FON) approach. The spin inversion leads the reaction pathway transferring from the triplet potential energy surface (PES) to the singlet's accompanying with the activation of the second C-H bond. The overall reaction is calculated to be exothermic by about 231 kJ mol^{-1}. Frequency and NBO analysis are also applied to confirm with the experimental observed data.

Keywords DFT fractional occupation number approach · Minimal energy crossing point · Potential energy surface · Spin-flip transitions · Zirconium and ethane reaction mechanism

Introduction

Owing to high potential economic and environmental significance, gas-phase reactions of transition metal (TM) atoms and their clusters with small alkanes and halomethanes are attractive to extensively investigate both experimentally and theoretically [1–9]. The activation of C-H (X) and C-C bonds of the hydrocarbons aroused by transition metals, with H-migration from C to the TM atoms forming the C-H insertion products were usually explained as the mechanisms of TM catalyst [10–36]. This type of reaction partially exists intersystem crossings under "spin-forbidden" transitions, involving several potential energy surfaces (PES) [37, 38] with different spins. In the two-state reactivity (TSR) [39] or multiple-state reactivity (MSR) [40–43], spin inversions may accelerate the reaction in the vicinity of a crossing region of different spin-symmetric states [44]. Because of the complexity of two-electron correlation and one-electron relativistic effects (spin-orbit coupling - SOC) [45, 46] in the TM atoms, how to locate the minimum energy crossing point (MECP) is a challenge for theoretical researchers.

At the nonrelativistic approximation level, two adiabatic PESs with different spin-symmetries of *N*-atom molecular system intersect at a 3*N*−7 dimensional subspace shaping the crossing seam that guides the reaction wave-packet to cross in a low energy crossing region (LECR) around the MECP, which represents a transition structure for a spin inversion under 3*N*−8 dimensions. The critical point of procedure is to determine the transition position, i.e., the crossing point between multiple-electronic states of spin multiplicities. A LECR of two different spin symmetry PESs may easily be achieved by the reacting wave packet through thermal activation, and that may outbalance a low nonadiabatic transition probability. Under the Born-Oppenheimer approximation processes, the spin inversion occurs by nonadiabatic coupling because of the inclusion of SOC. The MECP lies energetically somewhat below the LECR.

To determine the MECP in low energy crossing region is a challenge. There are some methods to overcome this dificullty [47–56]. Wave function multiple-configuration (e.g., MCSCF or CASSCF) and density functional theory (DFT) based procedures have been operated. A generic process is counting the energies and gradients of the two

Y. Xiao · X.-Y. Chen · Y.-X. Qiu · S.-G. Wang (✉)
School of Chemistry and Chemical Engineering, Shanghai Jiao Tong University, 200240 Shanghai, China
e-mail: sgwang@sjtu.edu.cn

different spin multiplicities simultaneously for a series of structures of the reaction complex. Then these data are treated by an interfaced subroutine, which will approach the crossing point step by step. In this work, we will adopt the fractional orbital occupation number (FON) DFT approach [57] suggested by us which is a simple validated approach for searching the MECP in the LECR [57–59].

To activate the C-H and C-C bonds has drawn much attention on experimental and theoretical works [10–36] due to their large bond energy. The energy to active these bonds can be substantially reduced by catalysts in which the TM complexes have a higher potential than others. Very meaningfully, Andrews and co-workers initiated novel insights into the reactions of TM atoms with electron-rich alkane-species [3, 5, 15–35]. An interested example of the fourth-row metal atoms + ethane reaction has been experimentally measured in the argon matrix by Andrews and coworkers [26]. They have suggested that the reaction pathway may exist intersystem crossing somewhere and assigned the products by using infrared spectroscopy and theoretical vibration frequency calculations. But there are still some open questions unsolved in this reaction. In this work, we want to investigate the reaction mechanism in detail, especially to demonstrate the interstate crossing mechanism. We will follow the reaction chain of (1),

$$\begin{aligned} &Zr + CH_3{-}CH_3 \rightarrow Zr{-}CH_3{-}CH_3\,(\mathbf{1}) \rightarrow ZrH{-}CH_2{-}CH_3\,(\mathbf{2}) \rightarrow \\ &ZrH_2{-}\,CH_2 = CH_2\;\;(\mathbf{3}) \rightarrow ZrH_3 - CH = CH_2\;\;(\mathbf{4}) \end{aligned} \qquad (1)$$

where the energies and structures of the various intermediates and transition points in both of triplet and singlet spin states will be determined, and then the MECP will be determined by FON-DFT [57] approach. Frequency and NBO analysis will also be calculated for all intermediate and product species.

Methodology

Most calculations were performed by relativistic DFT program of Amsterdam, ADF2010, which was initially developed by Baerends et al. [60–62] in this work. The localized spin density (LSD) with correlated potential of Vosko-Wilk-Nusair (VWN) [63] and the generalized gradient corrections for exchange correlation of Perdew and Wang (PW91) [64] were used in this work. The so-called all electron frozen core method was adopted in which the core electrons were calculated by the relativistic Dirac-Slater method [65] and then unchanged transferred into the molecules. All the valence electrons (out of the core shells of C($1s^2$) and Zr($1s^2$-$3d^{10}$)) were described by the standard triple-ζ Slater-Type-Orbital (STO) plus two sets of polarization functions (TZ2P) basis sets [66]. Due to relativistic effects of Zr, the zero-order regular approximation (ZORA) [67] scalar relativistic method were employed.

Harmonic vibrational frequencies and zero point energy corrections (ZPE) were analyzed by numerical differentiation of the energy gradients for all important products and intermediates and transition structures. In order to prove the reaction path correctness, the intrinsic reaction coordinate (IRC) [68, 69] procedure was used following in both directions (forward and backward) along the minimum energy path from the transition states to the most stable equilibrium structures.

For further interpretation, the natural bond orbital (NBO) [70] and Wiberg bond order (WBO) [71] analysis were performed by applying SDD [72] (with the relativistic effective core potential) basis set for Zr and 6-31G* [73] basis sets for the other atoms respectively at the B3PW91-DFT level with the help of the Gaussian03 [74] program.

Results and discussion

The reaction route simply obeys the principle of lowest energy. Table 1 presents the ZPE-corrected energies (relative to the ground state of ^{3}Zr and ethane) of each stationary and transition states both of the triplet and singlet spin states. The NBO, WBO and frequency analyses about the two major products ZrH_2-CH_2 = CH_2 and ZrH_3-CH = CH_2 of the rate-determining step with different spin multiplicities are presented in Table 2, where the experimental frequency from IR spectrum (in parenthesis) are well in agreement with ours.

Table 1 ZPE-corrected energies [a] (in kJ mol^{-1}) of intermediates, transition states and products relative to the ground state reactants Zr(^{3}F) + C_2H_6 in triplet and singlet spin states, respectively

Species	Triplet	Singlet
Zr: Zr + C_2H_6	d^2s^2 ^{3}F 0	d^2s^2 ^{1}D +78.3
1	−20.8	
$TS_{1/2}$	−17.7	
2	−167.3 (~ − 105[b])	−125.4
$TS_{2/3}$	−131.1	−114.0
3	−167.3	−265.9 (~ − 201[b])
$TS_{3/4}$	−61.6	−135.9
4	−101.3	−230.7 (~ − 184[b])
5	−57.4	
$TS_{5/6}$	41.5	
6	−58.5	
Zr + C_2H_4+ H_2	131.6	

[a] ZPE-corrected, from SO averaged ZORA-VPW91-TZ2P DFT

[b] The computational values at 6-311++G(3df,3pd)/SDD-B3LYP level by Andrews and cooperators[26] in bracket

Table 2 NBO, WBO and frequency (ν) data of the major products $ZrH_2CH_2{=}CH_2$ (**3**) and ZrH_3CHCH_2 (**4**) in the two spin states

Property	ZrH_2-CH_2 = CH_2		ZrH_3-CH = CH_2	
	^{3}**3**	^{1}**3**	^{3}**4**	^{1}**4**
q(C1) [a]	−0.67	−0.88	−0.61	−0.62
q(H2/H5/H6) [a]	0.26×3	0.25×3	0.25,0.25,0.19	0.25,025,0.22
q(H1/H3/H4) [a]	−0.38,0.26,−0.38	−0.37,0.25,−0.37	−0.001,−0.001,-0.37	−0.29,−0.31,−0.29
q(C2) [a]	−0.67	−0.88	−0.48	−0.43
q(Zr) [a]	1.07	1.48	0.77	1.21
C1 [b]	$2s^{1.09}$ $2p^{3.56}$	$2s^{1.14}$ $2p^{3.73}$	$2s^{1.17}$ $2p^{3.41}$	$2s^{1.17}$ $2p^{3.44}$
Zr [b]	$4d^{2.14}5S^{0.65}$	$4d^{1.92}$ $5s^{0.45}$	$4d^{2.47}$ $5s^{0.60}$	$4d^{1.93}$ $5s^{0.62}$
$\nu(H_2Zr/H_3Zr)$ [c]	H_2Zr:1582.9	H_2Zr:1597.8 (1562.8[e]), (1566.1[f])	H_3Zr:1563.0	H_3Zr: 1608 (1646.0[e]), (1591.2[f])
$\nu(C_2Zr)$ [c]	326.5	520.4(519.7[e]) (519.5[f])	557	597.9
ν(C-C) [c]	1226.3	960.8(993.2[e]) (958.8[f])		
ν(H-H) [c]			H-H:2984.8	
$WBO_{Zr\text{-}C1}$ [d]	0.44	0.83	0.84	0.86
$WBO_{Zr\text{-}C2}$ [d]	0.44	0.83	0.20	0.19
$WBO_{Zr\text{-}H3/4}$ [d]	H4:0.85	H4:0.86	H4:0.85	H3:0.88
$WBO_{Zr\text{-}H1}$ [d]	0.85	0.86	H1:0.25	H1:0.91
$WBO_{C1\text{-}C2}$ [d]	1.52	1.07	1.90	1.90
$WBO_{H\text{-}H}$ [d]			H1-H3::0.74	H1-H4:0.001

[a] Weinhold charge, [b] Weinhold electron configuration, [c] Frequency in cm^{-1}, [d] Wiberg bond order. [e] calculated values by Andrews [26], [f] experimental values by IR spectrum

The reaction path energies with two different spin states are plotted in Fig. 1. The most major geometric parameters for each stationary and transition points are shown in Fig. 2. The reactant Zr atom has the high-spin triplet ^{3}F ($4d^25s^2$) as the ground state and the intermediates **1** (Zr-CH_3-CH_3) and **2** (ZrH-CH_2-CH_3) also display the triplet ground states. However, the major products **3** (ZrH_2-CH_2 = CH_2) and **4** (ZrH_3-CH = CH_2) in a low-spin singlet state were found on Andrews and co-workers' experimental observations and from their B3LYP computations. They proposed a mechanism for the Zr + ethane reaction and suggested that the intersystem crossing should occur along the lowest energy path [26].

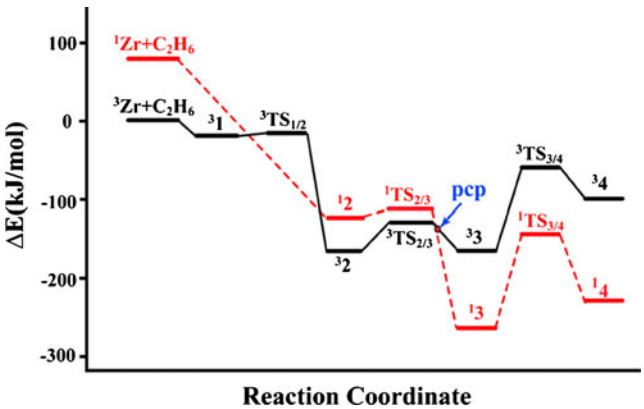

Fig. 1 Energy level along the reaction pathway $Zr + C_2H_6 \rightarrow ZrH_3$-CH = CH_2 in triplet and singlet spin states (ΔE in kJ mol^{-1})

Here, we suppose two reaction paths with different spin states (i.e., averaged out SOC), and regenerate the whole reaction path which is supplemented with many additional details, as shown in Figs. 1 and 2.

How to get correct atomic energy with different states of transition metal is still a challenge in DFT due to the multi-configuration effects. Zr with d^2s^2 configuration may have two lower states of ^{3}F and ^{1}D. Fortunately, "sum method" [75] of DFT may solve such problem. By using "sum method" these two states can be obtained reasonably. The energy difference of ^{3}F and ^{1}D is 78.3 kJ mol^{-1} which differs little from experimental value [76] 67.4 kJ mol^{-1} (not too much for open d-shell on DFT).

Triplet state of spin-conserved mechanism for Zr(^{3}F) with ethane reaction

The ground state of Zr atom is a triplet state of $^3F(4d^25s^2)$. Firstly, Zr atom moves to C_2H_6 forming a complex Zr-CH_3-CH_3 (^{3}**1**) with energy reduced of 29 kJ mol^{-1}. Crossing over the transition state ^{3}**TS$_{1/2}$** with a small energy barrier of 3 kJ mol^{-1} due to the Pauli repulsion of electronic cloud, Zr inserts into the H-C bond of C_2H_6. Meanwhile, the first hydrogen breaks away from C1 and migrates toward Zr forming the stationary ZrH-CH_2-CH_3 (^{3}**2**). In this step, the atomic distance between Zr and C1 decreases from 2.78 (^{3}**1**)

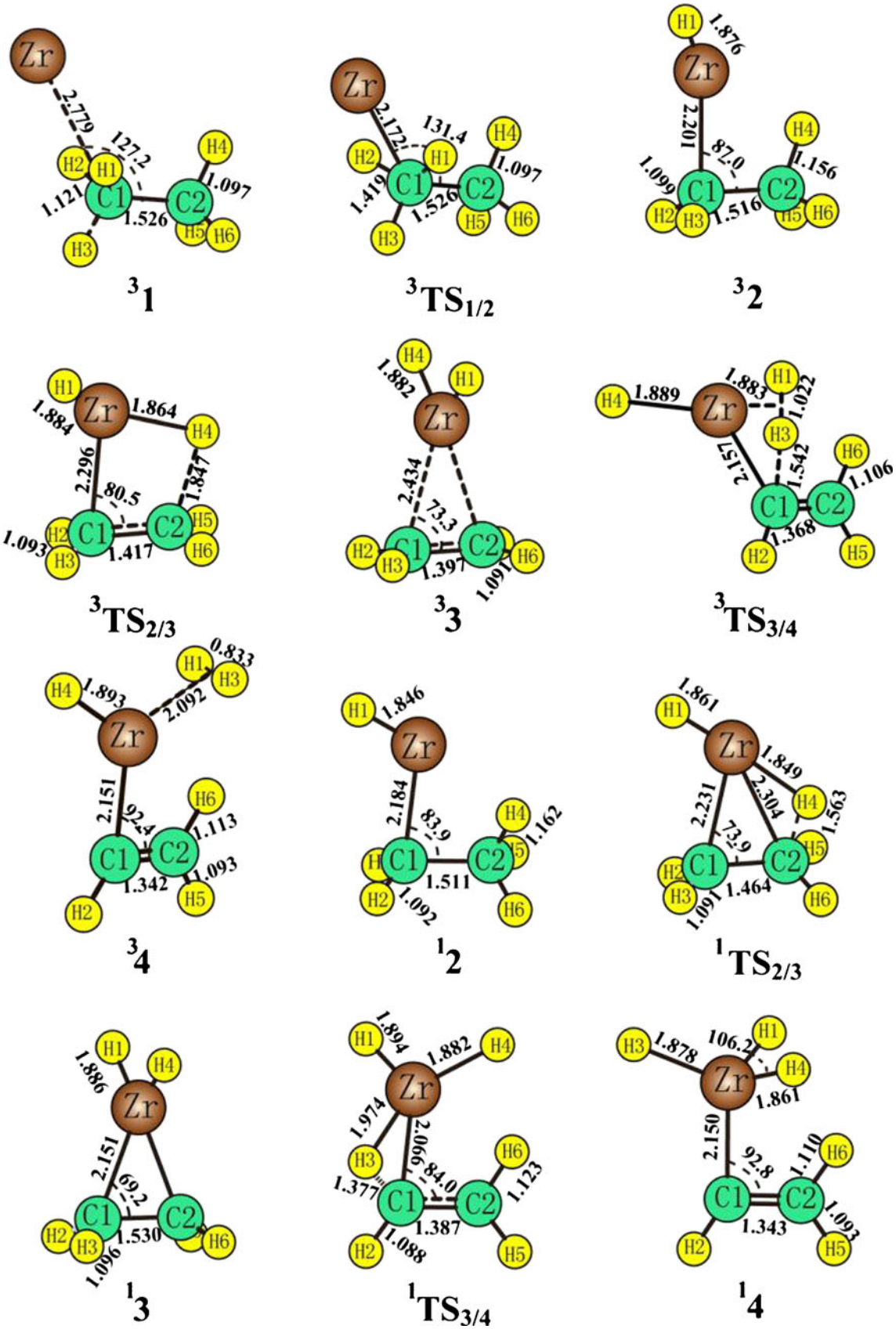

Fig. 2 Equilibrium geometries of intermediates, transition states and products in the Zr + C_2H_6 reaction with triplet and singlet states (bond length in Å, bond angle in °). The **2**, **3**, **4** structures in both spin states with C1, C2v, Cs symmetry, respectively, ^{3}**1** with symmetry Cs

to 2.20 (^{3}**3**) Å same as standard bond length of Zr-C. This reaction step of ^{3}**1** → ^{3}**2** is largely exothermic by 166 kJ mol^{-1}.

From the intermediate ^{3}**2**, Zr needs to attract the second hydrogen which moves from the other carbon (C2). The reaction proceeds to go through the transition state ^{3}**TS$_{2/3}$** with activation energy of 35 kJ mol^{-1}. Remarkably, the C2-H bond elongates to 1.85 Å from 1.16 Å in ^{3}**TS$_{2/3}$**, while the bond distance of Zr-H4 becomes 1.86 Å. It shows that the C2-H4 bond is broken and Zr-H4 bond is forming. Meaningfully, as compared to that in ^{3}**2**, the bond length of C1-C2 reduces by 0.1 Å which implies the tendency of the double bonds of C = C to be soon created. Then the H4 continues to move away from the C2 anticlockwise around Zr to form the C2v symmetry in ^{3}**3** (ZrH_2-CH_2 = CH_2) (see Fig. 2). Our IRC calculation on the PES from ^{3}**2** → ^{3}**3** demonstrates the transition state ^{3}**TS$_{2/3}$** connect the two ends of ZrH-CH_2-CH_3 (^{3}**2**) and ZrH_2-CH_2 = CH_2 (^{3}**3**) in the forward and backward directions, respectively.

Then, the third hydrogen (H3) moves toward top and interacts with H1 forming a 2H group, meanwhile H4 turns to the backside of Zr with a Cs symmetry at the transition state ^{3}**TS$_{3/4}$**. The notable activation barrier is about 106 kJ mol^{-1} due to the H3-C1 bond broken. The ^{3}**3** proceeding to product ^{3}**4** needs about 66 kJ mol^{-1} energy. It is interesting that in product ^{3}**4**, the two hydrogen atoms are not directly bonded with Zr but have a tendency to form a H_2 group (the H-H distance being only 0.83 Å) and weakly interact with Zr (the distance between H-H and Zr being 2.09 Å). Totally, the triplet reaction from ^{3}Zr + C_2H_6 to final species ^{3}**4** is exothermic by about 101 kJ mol^{-1}.

Singlet state of spin-conserved mechanism for Zr(^{1}G) with ethane reaction

Now, turn to the singlet reaction process. Different from that of triplet trajectory, we searched for the first corresponding complex **1** and the first transition state in singlet PES, but were unable to discover them. Thus, the first reaction step is a straight inserting the C-H bond by Zr with excited singlet state to form the intermediate ZrH-CH_2-CH_3 (^{1}**2**). Such situation also appeared in Re + CH_4 reaction [58]. The high-energy low-spin singlet ^{1}D term of Zr lies above its ^{3}F ground state by 78 kJ mol^{-1}. As compared to the tiny active barrier of 3 kJ mol^{-1} in triplet reaction path, the excited Zr (^{1}D) with high-potential could be supposed to overcome their negligible energy barrier directly arriving at the stationary ^{1}**2**. So this process is regarded as a barrierless reaction pathway. There is a large energy difference of 237 kJ mol^{-1} between the excited reactants ^{1}Zr + C_2H_6 and the stationary ^{1}ZrH-CH_2-CH_3.

After the complex ^{1}**2**, the singlet reaction pathway is similar to that of triplet state. The ^{1}**2** continues to go through the potential barrier of ^{1}**TS$_{2/3}$** by 11 kJ mol^{-1} to the intermediate ^{1}**3**. At the ^{1}**TS$_{2/3}$** state, the C2-H4 bond distance is 1.56 Å much larger than the standard C-H bond which means when H4 leaves C2 moves to Zr. This step ^{1}**2** → ^{1}**3** is largely exothermic by 140.5 kJ mol^{-1}. There is an obvious distinguishment of C1-C2 bond distance between ^{3}**3** and ^{1}**3** of 1.40 Å and 1.53 Å, respectively. The three-body ring geometric structure of ^{1}**3** makes it more stable than that in ^{3}**3**, about −99 kJ mol^{-1} lower than the triplet educt.

On the last step, the third hydrogen, H3, moves from C1 to Zr via transition state ^{1}**TS$_{3/4}$** (see Figs. 1 and 2). The H3 migrates toward Zr constructing a ZrH_3 group which quite differs from the triplet process. IRC investigation confirms the rearrangement process. From ^{1}**3** to ^{1}**4** step, it is endothermic by about 35 kJ mol^{-1} and with a transition barrier of 130 kJ mol^{-1}. The high activation barrier of ^{1}**TS$_{3/4}$** indicates the difficulty to take off H from the C-H bond. The ^{1}**4** is also expected as kinetically stable regardless of the presence of C = C double bonding. The high barrier of ^{1}**TS$_{3/4}$** which could be deemed to be the rate-determining step on the whole reaction path is much greater than that of ^{1}**TS$_{2/3}$** (6 kJ mol^{-1}). However, the whole reaction on singlet pathway is largely exothermic by about 309 kJ mol^{-1}.

Possible further reaction mechanism on singlet state to ethene

Although in Andrews's report [26] the ground state ^{3}**Zr** did not react with ethane due to the unobserved Zr(C_2H_4) which would be logical for H_2 elimination product in their experiment. After searching along the forward process of the reaction, the triplet Zr(C_2H_4) is found while the singlet reaction process is still stopped on ^{1}**4**. The further reaction pathway and intermediates structures are shown in Figs. 3 and 4. As mentioned above, in ^{3}**4**, Zr is very weakly interacted with H1-H3 group. When the 2H group escapes from Zr creating

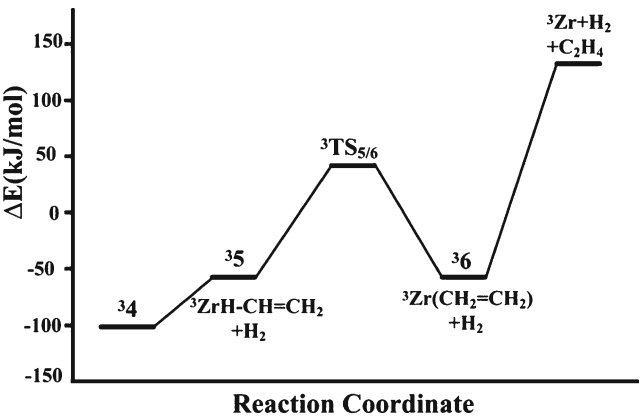

Fig. 3 Energy level along the further reaction pathway of $H_3Zr(C_2H_3)$ → Zr + H_2 + CH2 = CH_2 in triplet spin-state (ΔE in kJ mol^{-1})

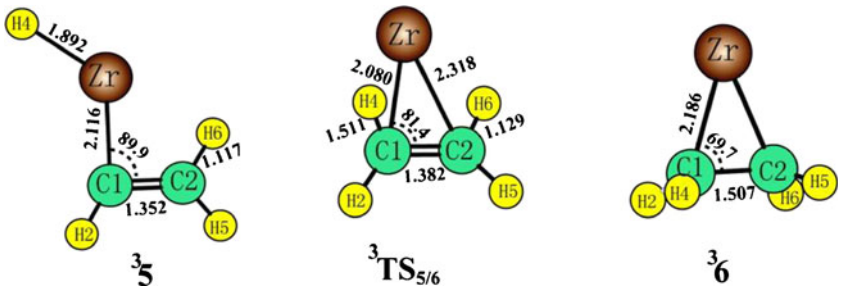

Fig. 4 Equilibrium geometries of intermediates, transition states and products in forth reaction of ZrH_3-CH = CH_2 → Zr + H_2 + CH2 = CH_2 in triplet spin-state (bond length in Å, bond angle in °)

^{3}ZrH-CH = CH_2 + H_2 (^{3}**5**), there will be no activation barrier and it is endothermic by about 44 kJ mol^{-1}. The H4 transfers from Zr to C1 crossing the transition state ^{3}**TS$_{5/6}$** with a barrier of 99 kJ mol^{-1} to form ^{3}Zr(CH_2 = CH_2) + H_2 (^{3}**6**). If the reaction still has onward process, Zr can leave ethene and the whole dehydrogenation reaction from ethane to ethene catalyzed by transition metal Zr may be finished. But the last step needs energy of 190 kJ mol^{-1} which hardly occurred.

Intersystem crossing and the conceivable overall reaction pathway

From above spin conserving (triplet or singlet state) reaction mechanism, one can see that the lowest energy of Zr atom and complex **1** and **2** are all in the triplet ground states, however the final products **3** and **4** are both in singlet states. So the low energy reaction path should not be fastened on one adiabatic PES, intersystem crossing might occur somewhere on the two PESs. The 3d-, 4d- and 5d-TM included reactions may refer to more than one adiabatic PES as indicated by some experimental and theoretical investigations [14, 15, 77–80]. From Fig. 1, it should be suggested that the reaction jump from triplet to singlet PES may be near the projected crossing point (PCP) between ^{3}**TS$_{2/3}$** and ^{1}**3**.

As a result, the reaction of laser ablated Zr with ethane starts from the formation of complex ^{3}**1** and continues to go to complex ^{3}**2** via a slender transition barrier ^{3}**TS$_{1/2}$** on the triplet PES. The interested step is from **2** to **3** via transition state **TS$_{2/3}$**. Although the second hydrogen H4 moves from C2 to Zr may form ZrH_2-CH_2 = CH_2 (^{3}**3**), complex ^{3}**2** and ^{3}**3** are equal in energy (by accident). But if ZrH_2-CH_2 = CH_2 (**3**) changes to singlet state ^{1}**3**, it will become more stable with 99 kJ mol^{-1} lower than in triplet state. Thermodynamically, the singlet complex **3** is much more favored than that in triplet. Thus, the triplet reaction may cross somewhere near the PCP region reaching the singlet trajectory between ^{3}**TS$_{2/3}$** and ^{1}**3**. However, the structures of the triplet and singlet are different geometrically except the reaction coordinate at PCP point. This will need some energy for the spin-flip process. Finally, the reaction path will get to ^{1}**4** via ^{1}**TS$_{3/4}$**. Overall, a conceivable lowest-energy reaction pathway of Zr atom + ethane with spin crossing is as follows:

$$\mathrm{Zr}\left(^3\mathrm{F}\right) + \mathrm{C_2H_6} \rightarrow {}^3\mathrm{Zr-CH_3-CH_3}\left(^3\mathbf{1}\right) \rightarrow {}^3\mathbf{TS_{1/2}} \rightarrow {}^3\mathrm{ZrH-CH_2-CH_3}\left(^3\mathbf{2}\right)$$
$$\rightarrow {}^3\mathbf{TS_{2/3}} \rightarrow \mathbf{PCP} \rightarrow {}^1\mathrm{ZrH_2-CH_2=CH_2}\left(^1\mathbf{3}\right) \rightarrow {}^1\mathbf{TS_{3/4}} \rightarrow {}^1\mathrm{ZrH_3-CH=CH_2}\left(^1\mathbf{4}\right).$$

In this instance, the symmetries of the structures of **1**, **2**, **3** and **4** belong to Cs, C1, C2v, Cs, respectively (see Fig. 2). The overall reaction which starts from the triplet PES and ends in the singlet PES at ^{1}**4** would be exothermic by ~231 kJ mol^{-1}.

Crossing points between the PESs of different spin multiplicities

As is well known, density functional theory does well in many equilibrium configurations by a single determinant wavefunction in most chemical systems. Always, the electronic configuration satisfies the "Aufbau principle", that means the occupied orbitals are lowest in energy than the unoccupied orbitals at DFT ground state which is proved by Janak [81]. However, in some near-degenerate configuration states, the empty orbital below the occupied orbital in energy always happens. Non-dynamic correlation effects become crucial. In such cases, multiple-configuration wave functional methods like MCSCF or CASSCF [48–56] based procedures should be adopted for the orientation of the transition region. Alternatively, we have suggested a simple DFT fractional orbital occupation number (FON) approach [57] to simulate the non-dynamical correlation effects for searching for the MECP in the LECR.

To better analyze the electronic configuration of spin crossing process, an energy level digram for frontier orbitals is plotted in Fig. 5. Among the six-pair frontier orbitals, four α and two β spin-orbitals and three α and three β spin

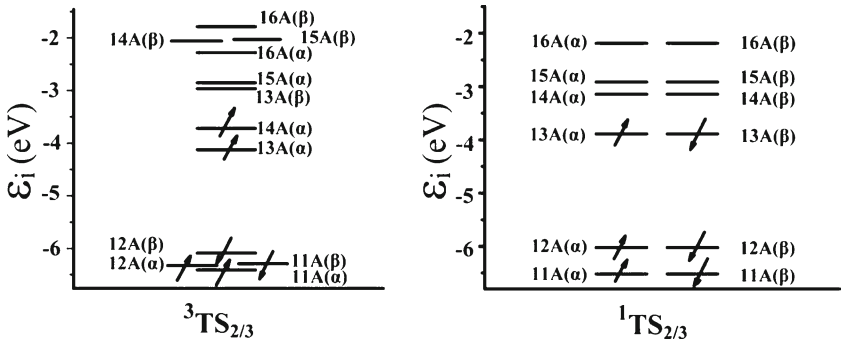

Fig. 5 The energy level diagram for frontier spin orbitals with the six HOMOs and six LUMOs in ^{3}**TS$_{2/3}$** and ^{1}**TS$_{2/3}$**, respectively (ε in eV)

orbitals are occupied in ^{3}**TS$_{2/3}$** and in ^{1}**TS$_{2/3}$**, respectively. The highest occupied molecular orbital (HOMO) is the 14Aα and the lowest unoccupied molecular orbital (LUMO) is 13Aβ in ^{3}**TS$_{2/3}$**. However, the HOMO in ^{1}**TS$_{2/3}$** is 13A (α + β), the LUMO is 14Aα. Clearly, from triplet to singlet states, it needs one electron from α transferring to β spin. Along with the spin-flip process, the 14Aα orbital energy increases and the 13Aβ orbital energy decreases until the two orbital energies become equal. At this moment, the "Aufbau principle" is obeyed in both electronic configurations of different spin-symmetry.

When spin inversion is carried out by nonadiabatic coupling over the LECR with a transition structure, two conditions should be fulfilled: one is the transition structure ought to be the lowest point energetically on the crossing seam where the classical trajectory may crosses with lowest energy; the second is the Franck-Condon principle, i.e., the energy of the two different spin symmetry should be the same, $E(^3\text{A}) = E(^1\text{A})$, for the identically transition structure.

As shown in Fig. 1, at the so called "projected crossing point" (PCP), $E(^3\text{A}) = E(^1\text{A})$, only the reaction coordinate $\angle_{\textbf{H4-Zr-C2}}$ (= 54.91°) is the same but with different partial geometric structures in a 3N-7 dimension (N=9-atomic system). However, the orientation of the PCP is only the first step, Franck-Condon principle is not fulfilled at the PCP.

Now, we start to apply FON-DFT method to determine the MECP. To optimize the fractional occupation number n of orbitals 14A$(\alpha)^n$ and 13A$(\beta)^{1-n}$ and simultaneously all of structure parameters except for $\angle_{\text{H4-Zr-C2}}$ taken as the constant value of 54.91° are optimized ensuring to locate at the lowest energy area. Changing with the n-variation (see Fig. 6b and c), orbital 14A$(\alpha)^n$ drops and 13A$(\beta)^{1-n}$ rises up. At n=0.425 point, the two orbital energies get equal. This optimized geometry is close to the MECP (see Fig. 6 left-bottom).

Then we need to check whether the transition structure is satisfied for Franck-Condon principle, that with the same structure should be $E(^3\text{A}) = E(^1\text{A})$. Occasionally it is needed to search once again (however it is a small probability event). There is only 0.69 kJ mol^{-1} energy difference which is within our convergent limitation between triplet and singlet states with the MECP structure.

Molecular structure and bonding

The major intermediates in the reaction of ethane dehydrogenation by Zr atom are **2**, **3** and **4**. Why in the later steps, the singlet spin state of **3** and **4** will become more stable than the triplet state? Now, we want to make more detailed analysis on the molecular structures on **3** and **4** with singlet and triplet spin states.

The optimized structures of **3** and **4** in both spin states are shown in Fig. 2. The harmonic vibrational frequencies (includes the experimental IR values), the values of Weinhold charge and Wiber bond order (WBO) are listed in Table 2. Compared with the experimental IR data, the DFT predicted vibrational frequencies of **3** and **4** in singlet spin states are matched much better than the triplet ones. For example, let's see ν(C-C) in ^{1}**3** and ^{3}**3**, the present DFT calculated values are 961 and 1226 cm^{-1}, respectively, and the experimental observable IR value is 959 cm^{-1} which is closer to the singlet ^{1}**3** than the triplet ^{3}**3**.

For ZrH_2-CH_2 = CH_2 (**3**), the Zr-C1 (same as Zr-C2 in C2v symmetry) bond distance is 2.43 Å and 2.15 Å and of C-C is 1.40 Å and 1.53 Å in the triplet and singlet states, respectively. The shorter the Zr-C bond length, the stronger the bond. And the elongation of C-C bond also contributes to the more stable three-ring structure in ^{1}**3**. From the natural bond orbital (NBO) analysis, the WBO of Zr-C for singlet (0.83) is nearly double of the triplet (0.44). The Weinhold charges of Zr and C in the two different spin states are 1.07 (Zr/^{3}**3**), 1.48 (Zr/^{1}**3**) and −0.67 (C/^{3}**3**), −0.88 (C/^{1}**3**), respectively, which tells us there is stronger ionic bonding between Zr-C in singlet than in triplet states.

For the ZrH_3-CH = CH_2 (**4**), there is about 129 kJ mol^{-1} energy difference between the two spin states although with nearly the same bond lengths of Zr-C and C-C. However, in ^{3}**4**, the Zr is connected to H1-H3 group in very weak attraction with 2.08 Å distance. The Weinhold charges of H1 and H3 are only −0.001 which means H1-H3 group is similar to a hydrogen molecule. In ^{1}**4**, Zr is bonded to 3H with ~1.87 Å bond lengths which is same as standard bonds. The three H-atoms (with charge of −0.3) are well-proportioned around Zr (with charge of 1.2) forming the more stabilized complex.

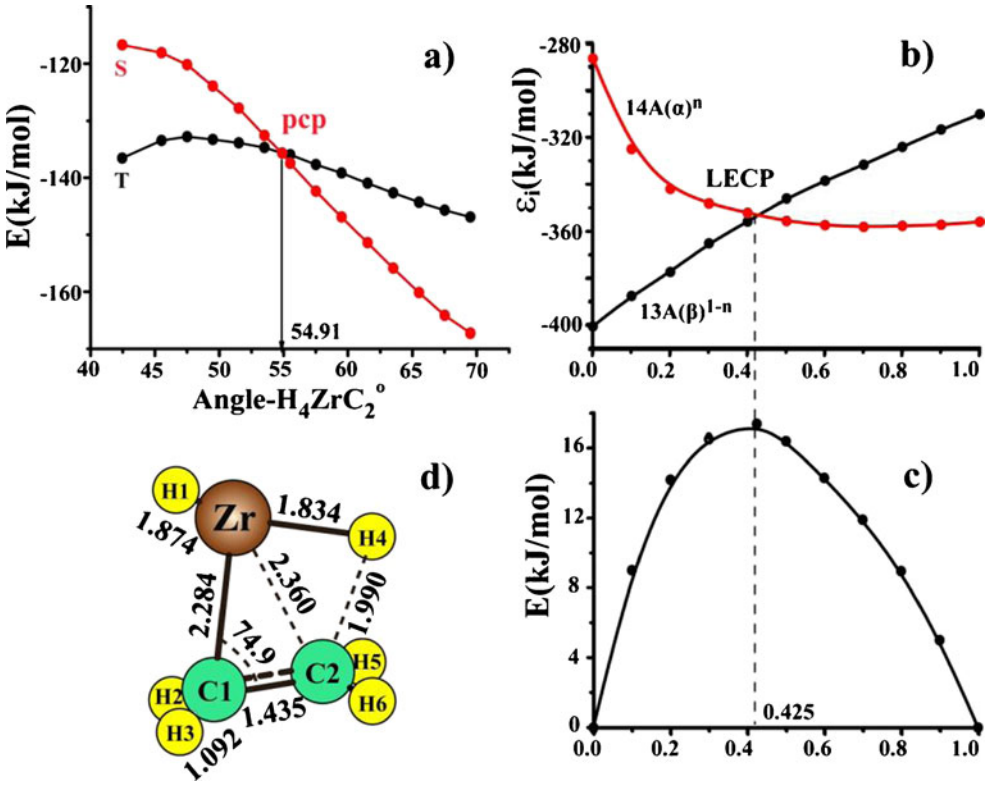

Fig. 6 a The optimized energy curve E along the reaction coordinate ∠H4-Zr-C2 between the transition state $\mathbf{TS_{2/3}}$ to ZrH_2-$(CH_2)_2$ (**3**) in the pure triplet and singlet spin states, respectively; (**b**) and (**c**): Under the DFT-FON procedure, the $14A(\alpha)^n$ and $13A(\beta)^{1-n}$ orbital energy curves versus FON n for mixed ensemble $n(^3A) + (1-n)(^1A)$ and the ensemble FON energy E; (**d**): Structural parameters of the MECP. E and ε_i in kJ mol^{-1}, bond lengths in Å, bond angles in degrees

So, ZrH_3-CH = CH_2 (**4**) in singlet state is more stable than in triplet.

Conclusions

In this paper we have theoretically investigated in detail ethane dehydrogenation in gas-phase by metal atom zirconium. At the relativistic DFT level, this reaction pathway has been studied on PESs both on triplet and singlet states. Some conclusions may be drawn as follows:

1. Along with the minimum energy reaction pathway of laser ablated Zr with ethane, two adiabatic PESs are included and spin inversion would occur somewhere. The available process contains four stationary states (**1** to **4**), three transition states ($\mathbf{TS_{1/2}}$ to $\mathbf{TS_{3/4}}$) and one spin inversion process. The integrated minimum energy reaction pathway may be described as follows:

$$\mathrm{Zr}\left(^3\mathrm{F}\right) + \mathrm{C_2H_6} \rightarrow {}^3\mathrm{Zr{-}CH_3{-}CH_3}\left(^3\mathbf{1}\right) \rightarrow {}^3\mathbf{TS_{1/2}} \rightarrow {}^3\mathrm{ZrH{-}CH_2{-}CH_3}\left(^3\mathbf{2}\right)$$
$$\rightarrow {}^3\mathbf{TS_{2/3}} \rightarrow \mathrm{PCP} \rightarrow {}^1\mathrm{ZrH_2{-}CH_2 = CH_2}\left(^1\mathbf{3}\right) \rightarrow {}^1\mathbf{TS_{3/4}} \rightarrow {}^1\mathrm{ZrH_3{-}CH = CH_2}\left(^1\mathbf{4}\right).$$

Starting from the Zr atom moves to C_2H_6 forming a complex of Zr-CH_3-CH_3 (^{3}**1**). Then the first dehydrogenation takes place following the H1 leaving from C1 to Zr forming the stationary ZrH-CH_2-CH_3 (^{3}**2**). Next, the second H4 goes away from C2 attracted by Zr which leads to the products ZrH_2-CH_2 = CH_2 (**3**). After the transition states of $\mathbf{TS_{2/3}}$, the singlet PES becomes lower than the triplet's. Between **2** and **3** there should be a region where the reaction crosses over the two PESs. Finally, the third H is migrated toward Zr from C1 forming the product of ZrH_3-CH = CH_2 (^{1}**4**).

2. The spin inversion occurs between the transition state $^3\mathbf{TS_{2/3}}$ and the product $^1ZrH_2$-CH_2 = CH_2 (^{1}**3**) near the saddle-points of two spin states with Zr inserting the second C-H bond. The spin crossing process brings to the product ^{1}**3** 99 kJ mol^{-1} lower energy than the corresponding triplet ^{3}**3**. The overall reaction starts from the triplet potential energy surface then passes through the MECP into the singlet potential energy surface and finally ends in the product ^{1}**4**. It would be exothermic by 231 kJ mol^{-1}.

3. The primary structures of the products ZrH_2-CH_2 = CH_2 (**3**) and ZrH_3-CH = CH_2 (**4**) both in triplet and singlet states are interpreted with the help of analysis by geometries, vibrational frequencies, the natural charges and bond orders. It is shown that the singlet products **3** and **4** are more stable than that of triplet.

Acknowledgments We acknowledge financial support by the National Nature Science Foundation of China (No. 20973109).

References

1. Yoshizawa K, Suzuki A, Yamabe T (1999) J Am Chem Soc 121:5266–5273
2. Bowers MT (1994) Acc Chem Res 27:324–332
3. Cho HG, Andrews L (2008) J Am Chem Soc 130:15836–15841
4. Arndtsen BA, Bergman RG, Mobley A, Peterson TH (1995) Acc Chem Res 28:154–162
5. Cho HG, Andrews L (2005) Angew Chem Int Ed 44:113–116
6. Roithova J, Schröder D (2010) Chem Rev 110:1170–1211
7. Eller K, Schwarz H (1991) Chem Rev 91:1121–1177
8. Armentrout PB (2001) Annu Rev Phys Chem 52:423–461
9. Irikura KK, Goddard WA (1994) J Am Chem Soc 116:8733–8740
10. Liu G, Zhao Y, Zhang W, Zhang X (2008) J Mol Struct (THEOCHEM) 869:75–80
11. Lv LL, Wang YC, Wang Q, Liu HW (2010) J Phys Chem C 114:17610–17620
12. Guo Z, Ke Z, Phillips DL, Zhao C (2008) Organometallics 27:181–188
13. Fedorov DG, Gordon MS (2000) J Chem Phys 112:10247–10258
14. Sievers MR, Armentrout PB (2003) Organometallics 22:2599–2611
15. Cho HG, Lyon JT, Andrews L (2008) J Phys Chem A 112:6902–6907
16. Cho HG, Andrews L (2006) Organometallics 25:4040–4053
17. Cho HG, Andrews L (2011) Dalton Trans 40:11115–11124
18. Cho HG, Andrews L (2011) Organometallics 30:477–486
19. Cho HG, Andrews L (2009) Organometallics 28:1358–1368
20. Cho HG, Andrews L (2009) Dalton Trans 30:5858–5866
21. Cho HG, Andrews L (2008) Organometallics 27:1786–1796
22. Cho HG, Lyon JT, Andrews L (2008) Organometallics 27:5241–5251
23. Cho HG, Andrews L, Vlaisavljevich B, Gagliardi L (2009) Organometallics 28:6871–6879
24. Cho HG, Andrews L, Vlaisavljevich B, Gagliardi L (2009) Organometallics 28:5623–5632
25. Cho HG, Andrews L (2010) Dalton Trans 39:5478–5489
26. Cho HG, Andrews L (2008) J Phys Chem A 112:1519–1525
27. Cho HG, Andrews L (2008) Eur J Inorg Chem. 2537–2549
28. Cho HG, Andrews L (2010) Organometallics 29:2211–2222
29. Cho HG, Andrews L (2008) Inorg Chim Acta 361:551–559
30. Cho HG, Andrews L (2010) J Phys Chem A 114:8056–8068
31. Cho HG, Andrews L (2004) J Phys Chem A 108:6294–6301
32. Cho HG, Andrews L (2004) Organometallics 23:4357–4361
33. Cho HG, Andrews L (2004) Inorg Chem 44:979–988
34. Cho HG, Andrews L (2004) J Am Chem Soc 126:10485–10492
35. Cho HG, Andrews L (2008) Inorg Chem 47:1653–1662
36. Koszinowski K, Schröder D, Schwarz H (2003) J Phys Chem A 107:4999–5006
37. Plattner DA (1999) Angew Chem Int Ed 38:82–86
38. Yarkony DR (1996) J Chem Phys 100:18612–18628
39. Schröder D, Shaik S, Schwarz H (2000) Acc Chem Res 33:139–145
40. Harvey JN, Poli R, Smith KM (2003) Coord Chem Rev 238:347–361
41. Gutlich P, Garcia Y, Goodwin HA (2000) Chem Soc Rev 29:419–427
42. Poli R, Harvey JN (2003) Chem Soc Rev 32:1–8
43. Gutlich P, Garcia Y, Woike T (2000) Coord Chem Rev 219:839–879
44. Poli R (2004) J Organomet Chem 689:4291–4304
45. Neese F, Petrenko T, Ganyushin D, Olbrich G (2007) Coord Chem Rev 251:288–327
46. Fedorov DG, Koseki S, Michael W, Gordon MS (2003) Int Rev Phys Chem 22:551–592
47. Chachiyo T, Rodriguez JH (2005) J Chem Phys 123:094711–094720
48. Jensen F (2003) J Chem Phys 119:8804–8808
49. Barbatti M, Ruckenbauer M, Lischka H (2005) J Chem Phys 122:174307–174316
50. Cui Q, Morokuma K (1997) Chem Phys Lett 272:319–327
51. Schoeneboom J, Thiel W (2004) J Am Chem Soc 126:4017–4034
52. Jensen F (1992) J Am Chem Soc 114:1596–1603
53. Miller WH, Handy NC, Adams JE (1980) J Chem Phys 72:99–112
54. Guo Z, Ke Z, Phillips DL, Zhao C (2007) Organometallics 27:181–188
55. Øiestad EL, Harvey JN, Uggerud E (2000) J Phys Chem A 104:8382–8388
56. Koga N, Morokuma K (1985) Chem Phys Lett 119:371–374
57. Wang SG, Chen XY, Schwarz WHE (2007) J Chem Phys 126:124109–124117
58. Li J, Chen XY, Qiu YX, Wang SG (2009) J Phys Chem A 113:8471–8477
59. Li Q, Qiu YX, Chen XY, Schwarz WHE, Wang SG (2012) Phys Chem Chem Phys 14:6833–6841
60. Baerends EJ, Ellis DE, Ros P (1973) Chem Phys 2:41–51
61. Velde G, Baerends EJ (1992) J Comput Phys 99:84–98
62. Ziegler T, Rauk A, Baerends EJ (1977) Theor Chim Acta 43:261–271
63. Vosko SH, Wilk L, Nusair M (1980) Can J Phys 58:1200–1211
64. Perdew JP, Chevary JA, Vosko SH, Jackson KA, Pederson MR, Singh DJ, Fiolhais C (1992) Phys Rev B 46:6671–6687
65. Rosen A, Lindgren I (1968) Phys Rev 176:114–125
66. Lenthe EV, Baerends EJ (2003) J Comput Chem 24:1142–1156
67. Lenthe EV, Baerends EJ, Snijders JG (1994) J Chem Phys 101:9783–9793
68. Deng L, Ziegler T (1994) Int J Quant Chem 52:731–765
69. Deng L, Ziegler T, Fan L (1993) J Chem Phys 99:3823–3836
70. Reed AE, Curtiss LA, Weinhold F (1988) Chem Rev 88:899–926
71. Wiberg KB (1968) Tetrahedron 24:1083–1096
72. Andrae D, Haeussermann U, Dolg M, Stoll H, Preuss H (1990) Theor Chim Acta 77:123–141
73. Ditchfield R, Hehre WJ, Pople JA (1971) J Chem Phys 54:724–732
74. Frisch MJ, Trucks GW, Schlegel HB, Scuseria GE, Robb MA, Cheeseman JR, Montgomery JA Jr, Vreven T, Kudin KN, Burant JC, Millam JM, Iyengar SS, Tomasi J, Barone V, Mennucci B, Cossi M, Scalmani G, Rega N, Petersson GA, Nakatsuji H, Hada M, Ehara M, Toyota K, Fukuda R, Hasegawa J, Ishida M, Nakajima T, Honda Y, Kitao O, Nakai H, Klene M, Li X, Knox JE, Hratchian HP, Cross JB, Bakken V, Adamo C, Jaramillo J, Gomperts R, Stratmann RE, Yazyev O, Austin AJ, Cammi R, Pomelli C, Ochterski JW, Ayala PY, Morokuma K, Voth GA, Salvador P, Dannenberg JJ, Zakrzewski VG, Dapprich S, Daniels AD, Strain MC, Farkas O, Malick DK, Rabuck AD, Raghavachari K, Foresman JB, Ortiz JV, Cui Q, Baboul AG, Clifford S, Cioslowski J, Stefanov BB, Liu G, Liashenko A, Piskorz P, Komaromi I, Martin RL, Fox DJ, Keith T, Al-Laham MA, Peng CY, Nanayakkara A, Challacombe M, Gill PMW, Johnson B, Chen W,

Wong MW, Gonzalez C, Pople JA (2003) Gaussian 03, revision B3. Gaussian Inc, Pittsburgh
75. Baerends EJ, Branchadell V, Sodupe M (1997) Chem Phys Lett 265:481–489
76. NIST Chemistry Webbook, NIST Standard Reference Data Base Number 69, http://physics.nist.gov/PhysRefDate/Handbook/Tables/rheniumtable5.htm
77. Si Y, Zhang W, Zhao Y (2012) J Phys Chem A 116:2583–2590
78. Li FX, Zhang XG, Armentrout PB (2006) Int J Mass Spectrom 255:279–300
79. Sändig N, Koch W (1997) Organometallics 16:5244–5251
80. Russo N, Sicilia E (2001) J Am Chem Soc 123:2588–2596
81. Janak JF (1978) Phys Rev B 18:7165–7173